Nuclear Instruments and Methods in Physics Research B 269 (2011) 1887–1891

Contents lists available at ScienceDirect

Nuclear Instruments and Methods in Physics Research B

journal homepage: www.elsevier.com/locate/nimb

Electron track analysis for damage formation in bio-cells

Y. Yoshii [a], K.L. Sutherland [b], H. Date [c,*]

[a] Education and Instrumentation Center, Sapporo Medical College, Sapporo 060-8556, Japan
[b] Department of Medical Physics and Engineering, Hokkaido University Graduate School of Medicine, Sapporo 060-8638, Japan
[c] Faculty of Health Sciences, Hokkaido University, Sapporo 060-0812, Japan

ARTICLE INFO

Article history:
Received 25 December 2010
Received in revised form 19 March 2011
Available online 30 May 2011

Keywords:
Electron track
Monte Carlo simulation
Aggregation index
Ionization cluster

ABSTRACT

The track structure of electrons generated in bio-tissues exposed to X-rays (or other radiation particles) is essential to cell damage. This paper reports on Monte Carlo track simulations of electrons to determine the degree of concentration of ionization and excitation events as the aggregation index (AI). AI is expected to correlate with the number of lesions in a cell nucleus, such as double-strand breaks (DSBs), which may lead to lethality of cells. The simulation results show that AI as a function of electron energy has a peak in low energy (sub-keV) regions and the induction of the lesions may be attributed to the ionization and excitation clusters generated in the tissues. The track pattern, associated with the primary track and secondary branch tracks, is also illustrated by counting the number of the branching points given by the ionization.

1. Introduction

Photon beams and heavy charged particles incident on living organisms produce many secondary electrons with low energies (sub-keV). These electrons play an important role in causing radiation damage to cells (e.g., [1–4]). For evaluating the energy transfer of radiation, the linear energy transfer (LET), i.e., energy transfer per unit length, has been used. The LET for electrons is averaged over the (typical) track. However, as is the case with heavy charged particles (known as the "Bragg peak"), an electron transfers most of its energy to the ambient medium around the end of the track, which is limited in space due to large cross sections of collisions (in low-energies) with molecules in the medium both for inelastic and elastic processes. This end region process results in the clustering of ionization and excitation events [4,5].

Lethal damage of cells has been recognized to occur as a consequence of unrepaired or certain misrepaired double-strand breaks (DSBs) of DNA in the cell nucleus (e.g., [6]). It may be reasonable to envisage that DSBs are yielded efficiently by spatially localized ionization events (i.e., clusters) [7–12]. The conventional classification of electron tracks consists of "spurs", "blobs", "short tracks" and "branch tracks", which are named for track patterns depending on the electron energy [4]. The former two terms may render the cluster of ionization and excitation events, while the latter two must contain several clusters. In any case, the clusters will create strand breaks of DNA in local volume with high probabilities. Therefore, it is of primary importance to know the clustering patterns of ionization and/or excitation events in the cell nucleus for investigating the damage of the cells exposed to radiation. For investigating the clustering nature associated with electron interactions, track simulations by the Monte Carlo method have been performed by many investigators [4,13–16], while the experimental evidence has been reported [5,17,18]. However, the correspondence between cluster properties and degree of physicochemical damage is still not well known. Further investigations are necessary to make clear the properties of electron tracks and size of the clusters important for creating lesions in cell nucleus.

In this paper, the track analyses concerning the localization of energy deposition and the branching pattern of electron tracks by Monte Carlo simulations are presented. A characteristic parameter for describing the ionization and excitation processes is introduced as the aggregation index (AI). The simulation results show clear evidence of the intense effect on the cell nucleus at the track end.

2. Methods

2.1. Monte Carlo simulation code of electrons

The Monte Carlo simulation code for electron tracks used in this study is the same as that of a previous paper [19]. In the code, three collision types: elastic, excitation and ionization, are taken into account in liquid phase water. The event-by-event algorithm is employed for tracing every electron with energy from a starting energy (below 10 MeV) down to below the cutoff energy (8.22 eV, the electronic excitation threshold). As a benchmark test, the average path length per electron track by the Monte Carlo

* Corresponding author. Address: N12-W5, Kita-ku, Sapporo 060-0812, Japan. Tel.: +81 11 706 3423; fax: +81 11 706 4916.
E-mail address: date@hs.hokudai.ac.jp (H. Date).

0168-583X/$ - see front matter © 2011 Elsevier B.V. All rights reserved.
doi:10.1016/j.nimb.2011.05.028

simulation has been compared with the CSDA (continuous slowing-down approximation) range of ICRU report 37 (1984) [20]. Although the path length (as a summation of length between collision events) and the CSDA range are not strictly identical, very good agreement between them (generally within 5% difference) has been confirmed for a wide range of electron energies from 20 eV to 10 MeV. In the computation of the path length, the primary electron was tracked after each branching point at the ionization event. Here, the primary electron means the higher energy electron of the two after the ionization, and the path length of low energy electrons below 10 eV is assumed to equal the thermalization distance given in ORNL/TM-10851 (1988) [21].

2.2. Aggregation index (AI) as a function of electron initial energy

Conventionally, the linear energy transfer (LET) has been cited as a fundamental quantity in the physical stage of radiation interaction with materials. The LET is essentially equivalent to the collision stopping power. The numerical integration of the reciprocal of the stopping power from the energy E of the starting particle down to zero energy gives the CSDA range, which is approximately equal to the path length. Since the CSDA range (or path length) provides us with a rough estimation how the particle with energy E travels afterward, it is referred to as "residual range" of the particle with energy E. If the LET as a function of the particle energy is replotted as a function of the residual range, we can see the average rate of the energy transfer as a function of the material depth the particle penetrates at maximum. It can be inferred that the energy transfer from electrons to water occurs significantly in a local area, within about 1 μm at low energies below 5 keV, which is analogous to the Bragg peak. It should be noted that the material dimension affected around the end region is confined to a shorter range than the residual range of electrons due to their tortuous motion [22,23]. Since a typical diameter of the nucleus in mammalian cells is around 5 μm, it is reasonable to suppose that damage (e.g., DSBs) is induced in the nucleus when the end region of the electron track coincides with the DNA structure in chromosomes.

In order to consider quantitatively the clustering of ionization and/or excitation events, the authors have investigated the distribution of length between two arbitrary locations of the events by using the Monte Carlo code [24]. Based on the assumption that a couple of the events occurring in a short distance less than about 3.4 nm (equivalent to the length of 10 bp in DNA strand) can cause double-strand breaks (DSBs) of DNA, the summation of the length distribution over a certain range (0–3 nm or 0–10 nm) was obtained, which we call "aggregation index (AI)". For example, the AI for 0–3 nm means the number of combination of events (ionizations and/or excitations) occurring within 3 nm distance, which is expected to be proportional to the DSB induction probability. Since it has been affirmed that the "intertrack" breaks of DNA in a few nanometers of distance by multiple tracks hardly occur even at therapeutic doses (up to 6 Gy by linac 6 MV), the AI was calculated for an isolated track as a function of the initial energy of electron as $AI(E_{in})$ in the present study.

For n (>1) events of ionizations and excitations, AI value falls in the range between 0 and $n(n-1)/2$, and we define its unit as "links" hereafter. In the conventional research for radiation effects, the DNA damage has been quantitatively represented by the yield (Y) as the number of DSBs in unit mass per dose (Gy). It can be shown that Y is nearly equal to the number of DSBs per keV as follows,

$$Y\left[\frac{10^{-11}\cdot \mathrm{DSBs}}{\mathrm{Gy}\cdot \mathrm{Da}}\right] = \frac{10^{-11}}{\frac{10^{-3}}{1.6\times10^{-19}}\times\frac{10^{-3}}{6.02\times10^{23}}}\times Y\left[\frac{\mathrm{kg}\cdot \mathrm{DSBs}}{\mathrm{keV}\cdot \mathrm{kg}}\right] = 0.9632\times Y\left[\frac{\mathrm{DSBs}}{\mathrm{keV}}\right] \cong Y\left[\frac{\mathrm{DSBs}}{\mathrm{keV}}\right] \quad (1)$$

On the assumption that AI per initial electron energy is proportional to Y, we have the next relations:

$$Y\left[\frac{\mathrm{DSBs}}{\mathrm{keV}}\right] = k\cdot\frac{\mathrm{AI}}{E_{in}}\left[\frac{\mathrm{links}}{\mathrm{keV}}\right] \quad (2)$$

$$k = \frac{Y\cdot E_{in}}{\mathrm{AI}} = \frac{y}{\mathrm{AI}}\left[\frac{\mathrm{DSBs}}{\mathrm{links}}\right] \quad (y[\mathrm{DSBs}] = Y\cdot E_{in}) \quad (3)$$

Here, k is a proportional factor, and it is determined by a comparison between y and AI.

2.3. Branching structure of electron tracks

As mentioned in the prior subsection, the ionization and excitation clusters to yield the damage are presumed to occur mainly in a sub-micron domain inside the nucleus (typically around 5 μm in diameter), which is generated by electrons with energies below a few keV at the end of the track trajectory. Since the end regions forming clusters arise also in secondary electron tracks, we have to consider a tree structure for the track. The number of the secondary electron tracks can be estimated by counting branch points (of the track) where ionization process produces a secondary electron with energy above a certain threshold (hereafter referred to "branching energy, E_c"). This branching energy, E_c, categorizes the size of the secondary track after the branching point (shown later in Fig. 3a). For example, "Ctrack-1 keV" means the track formed by an electron with energy above 1 keV, which undergoes 1 keV electron processes once for all. The secondary electron energy is determined using the algorithm by Grosswendt and Waibel (1978) [25] in the present Monte Carlo code. The algorithm tells us that the ratio of imparted energy to the secondary electron is very small compared with that of the primary electron, and this tendency increases with electron energy before the ionization collision.

2.4. Considerations of radical's behavior

As to the radicals produced at the ionization and excitation events, their behavior can be estimated by the thermal diffusion and the annihilation process by chemical reactions. In pure liquid water (aqua pura), radicals (i.e., $OH^{\cdot}$, e^{-}_{aq}, H_3O^{+}, etc.) may be mobile up to above 100 nm in 10^{-6} s [23,26]. However, their actual diffusion lengths have been known to be less than 10 nm in the real ambient condition in the cell where radical scavengers are present and targets for radical reactions lie [12,16,27–29]. For this reason, we can assume that the radicals stick around the original locations (i.e., the ionization and excitation points) within 10 nm. The physical processes including the radical diffusion last within microsecond order while repairing time of the lesion in cell nucleus is on the order of one minute to many hours [30]. Therefore, the damage and the repair processes are regarded as completely separable processes with respect to time-domain.

3. Results and discussion

3.1. Aggregation index (AI) per track

The curves in Fig. 1 represent AI (links) as a combination of numbers of two arbitrary events occurring within 0–3 nm and 0–10 nm lengths per one track. Each point plotted in the figure was obtained by averaging over more than several tens of tracks (the number differs according to energy, E_{in}, to get an equivalent precision, typically within ±1% in this calculation).

Fig. 2a shows AI per track for the initial electron energy in comparison with the DSB yield (y) for the initial electron energy. The

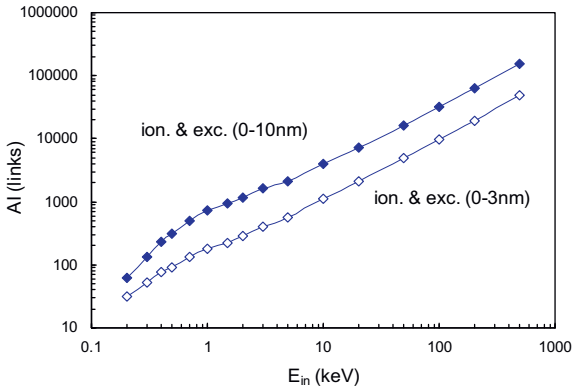

Fig. 1. Aggregation index (AI) per track for distances 0–3 nm and 0–10 nm between events as a function of initial electron energy, E_{in}. AI was calculated by the integration of the distance distribution for all combinations between the ionization and excitation points (from 0 to 3 nm and from 0 to 10 nm).

set of DSB yield data used here is the result of a Monte Carlo simulation by Friedland et al. (1998) [31], which has taken account of the chromatin structure of DNA. Here, AI value was multiplied by a factor of *k*, which was determined by the least square method so as to fit well to the yield. The same comparison between both values divided by the initial energy is shown in Fig. 2b. It is noted that the peak of AI/E_{in} appears at around the same energy as the yield (Y), as shown in Fig. 2b. The experimental evidence similar to this DSB yield curve was reported by Grosswendt (2005) [32]. The good agreement of the results in Fig. 2 suggests that AI can be a measure to estimate the DSB production rate. From the multiplication factor

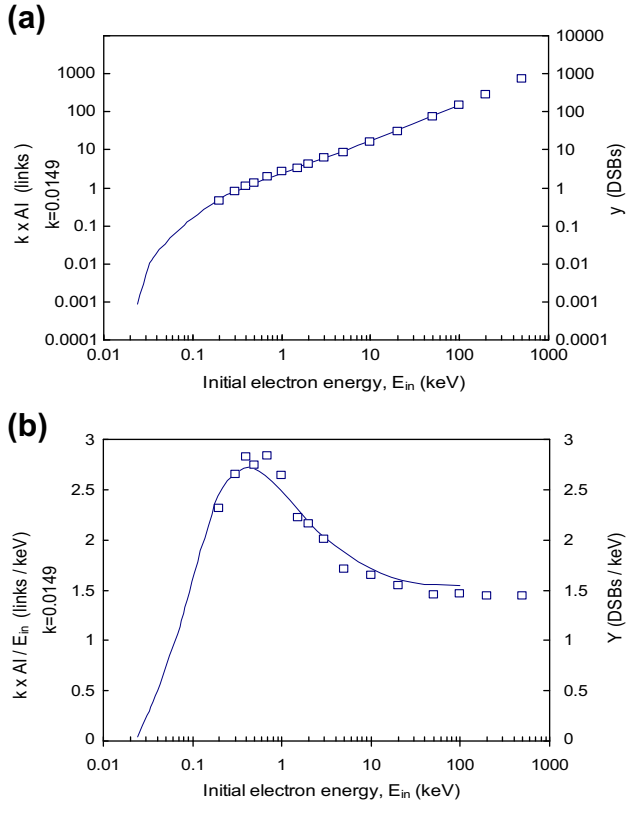

Fig. 2. (a) Comparison between AI for distances 0–3 nm and DSB yield (y) [31] as a function of initial electron energy, E_{in}. Square symbols represent AI and solid line DSB yield (y). Here, AI is multiplied by *k* factor (=0.0149). (b) Comparison between AI for distances 0–3 nm per initial electron energy and DSB yield per initial electron energy (Y) [31]. Square symbols represent AI and solid line DSB yield (Y). Here, AI is multiplied by *k* factor (=0.0149).

$k = 0.0149$, we can interpret one DSB to be produced by AI = 67 on the average, and the effect of radical species on the DSB production may be included in this multiplication factor. This result strongly supports the assumption that the clustering events (particularly, around the end of electron tracks) cause damage locally in the nucleus.

3.2. Number of secondary tracks per initial electron

Fig. 3b shows the number of branch tracks ("Ctracks") per primary electron as a function of initial electron energy. The branching energy (E_c) of secondary electrons at ionization points for counting the Ctrack was set to be from 500 to 1 MeV. It is noted that the Ctrack number is not proportional to the electron energy at the starting point of the track. This is because the electron energy is not evenly imparted to secondary electrons at each ionization event in the track, which is recognized from the algorithm used in the Monte Carlo code [25]. From observations of the track structure in three-dimensions, the main track of the primary electron leaves a long trace creating short branches sporadically. The number and energy distribution of the secondary electrons that create such branches were calculated for some initial electron energies as shown in Fig. 4. The distribution in Fig. 4 was obtained by averaging over 1000–2000 tracks. Interestingly, the secondary electron number per primary electron seems to follow a "power law" with respect to electron energy. We can see the production of secondary electrons is proportional to $SE^{-2.2}$ (SE: secondary electron energy).

As was shown in the AI analysis, the ionization and excitation cluster by the electron with energy below a few keV is important. The effective cluster size may be roughly estimated to be less than 0.1 μm in diameter from the view point of the residual range of ICRU report 37 (1984) [20]. Suppose that such a cluster is formed by the electron having energy below around 1 keV. The number

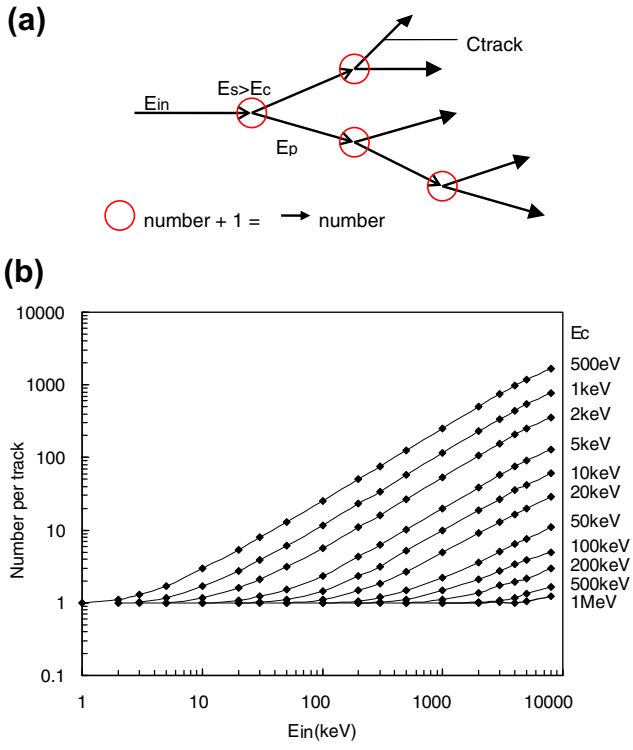

Fig. 3. (a) Schematic diagram of electron track structure for counting the number of tracks. The number of Ctracks is counted as the number of circles plus one. (b) Ctrack number per primary track as a function of initial electron energy, E_{in}. Here, the number includes the primary track.

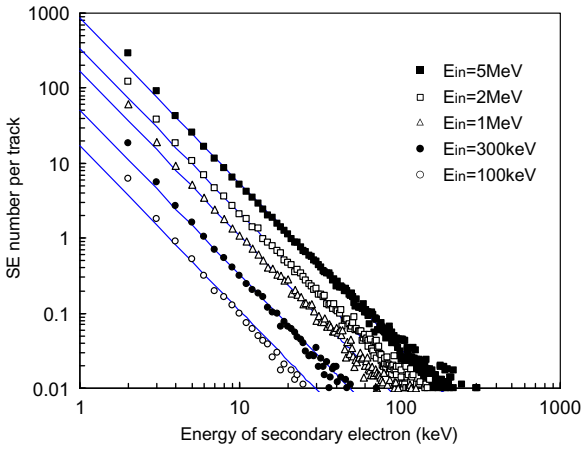

Fig. 4. Number of secondary tracks (per primary track) as a function of secondary electron energy. Solid lines represent a power law.

of tracks to yield this size of the cluster (i.e., the number of Ctrack-1 keV) is not as many as expected by the initial energy of the electron, as shown in Fig. 3b. For example, the average number of Ctrack-1 keVs for 15 keV is 2 while the primary electron with 15 keV can move up to above around 5 μm of total path length [20]. Therefore, multiple Ctrack-1keVs may occur along the primary track, but only two at most, inside the same nucleus.

The number of tracks per unit volume for X-ray irradiation can be determined by the energy distribution of initial electrons generated by photon interactions, that is, by the energy spectrum of the X-ray exposure. The cluster number density is not uniform in the volume of micrometer scale. However, if the tracks which cause the clusters are assumed to be located randomly, we can employ the Poisson statistics for estimating the number of lesions (e.g., DSBs) in the nucleus.

3.3. Absorbed dose and cluster number density

The absorbed dose by X-ray irradiation is equivalent to the summation of the initial energy of electrons produced in unit volume of the material, when the equilibrium state of electrons is sustained and the energy loss by the bremsstrahlung is negligible. Even under the same absorbed dose condition, the cluster number may vary according to the energy distribution of the initial electrons. However, the aggregation index (AI) for each track can be a comprehensible and effective measure because AI reflects directly the concentration degree of events probable to cause DNA damage, and we can evaluate the concentration effect of the events depending on the initial electron energy by multiplying the weight given in Fig. 2, which seems to be quantitatively correlated with the number of double-strand breaks (DSBs). Recently, the experimental technique to observe DSBs of DNA has been highly developed by using immunocytochemistry (e.g., [33–38], where the lesion (DSB) can be observed as fluorescent foci. By taking the precise irradiation condition of X-rays into account, the quantitative relationship among the DSB foci number, the incident photon beam density (yielding absorbed dose, D) and AI for the electron track would be made clear.

3.4. On extension of AI to proton (and other heavy charged particle) beams

In the present analysis, only electron tracks (generated by photon irradiation) were considered. However, the approach to take account of the ionization and excitation clusters in the electron track is available also for proton and other heavy charged particle beams. For example, the frequency of ionization collision along the proton beams in water is above 300 per μm for the energy from 1 to about 20 MeV (this energy range contributes to form the Bragg peak) [39]. The electrons produced in the ionization process (δ-rays) along the beam have energies below about 45 keV (i.e., 20 MeV/458). The aggregation index (AI) can be obtained for all ionization and excitation events by both the primary protons and electrons. The effect of the clustering may be divided into two parts: one for the events by the primary protons and the other for those by the electrons as indirect processes [40]. This leads to the difference of RBE or w_R (radiation weighting factor) between protons and electrons.

4. Conclusion

In this study, the probability of cell damage by exposure to photon irradiation was investigated by using the Monte Carlo simulation technique. The electron track properties were analyzed focusing on the aggregation degree of the ionization and excitation events and the track number in bio-cells. As a measure to evaluate the damage to the cell nucleus, the aggregation index (AI) per electron track was calculated for a variety of energies. The results suggest that AI per electron initial energy is appreciably correlated with the DSB yield in the conventional study. It was estimated that one DSB is produced by AI of 60–70 (links) for 0–3 nm. In addition to the AI analysis, the characteristics of electron track tree structure including the branch tracks were clarified as a function of the initial electron energy. The secondary electron number per primary electron was shown to follow a power law with respect to the secondary electron energy.

Acknowledgement

This work was financially supported by the Grant-in-Aid for Scientific Research in Japan.

References

[1] Y.-K. Kim, Energy distribution of secondary electrons I consistency of experimental data, Radiat. Res. 61 (1975) 21–35.
[2] R.N. Hamm, H.A. Wright, R. Katz, J.E. Turner, R.H. Ritchie, Calculated yields and slowing-down spectra for electrons in liquid water: implications for electron and photon RBE, Phys. Med. Biol. 23 (6) (1976) 1149–1161.
[3] J.E. Turner, J.L. Magee, H.A. Wright, A. Chatterjee, R.N. Hamm, R.H. Ritchie, Physical and chemical development of electron tracks in liquid water, Radiat. Res. 96 (1983) 437–449.
[4] H.G. Paretzke, D.T. Goodhead, I.G. Kaplan, M. Terrissol, Track structure quantities, IAEA-TECDOC 799 (1995) 633–721. Chapter 9.
[5] B. Grosswendt, Formation of ionization clusters in nanometric structures of propane-based tissue-equivalent gas or liquid water by electrons and α-particles, Radiat. Environ. Biophys. 41 (2002) 103–112.
[6] M.N. Cornforth, J.S. Bedford, A quantitative comparison of potentially lethal damage repair and rejoining of interphase chromosome breaks in low passage normal human fibroblasts, Radiat. Res. 111 (1987) 385–405.
[7] A.M. Kellerer, A generalised formulation of microdosimetric quantities, Radiat. Prot. Dosim. 31 (1990) 9–16.
[8] H.H. Rossi, M. Zaider, Elements of microdosimetry, Med. Phys. 18 (6) (1991) 1085–1091.
[9] D. Harder, R.P. Virsik-Peuckert, E.R. Bartels, Theory of intratrack pairwise lesion interaction, Radiat. Prot. Dosim. 52 (1994) 13–16.
[10] H.H. Rossi, Geometric domains in cellar radiobiology, Radiat. Prot. Dosim. 52 (1994) 9–12.
[11] T. Elsässer, M. Scholz, Improvement of the local effect model (LEM) – implications of clustered DNA damage, Radiat. Prot. Dosim. 122 (2006) 475–477.
[12] T. Elsässer, M. Scholz, Cluster effects within the local effect model, Radiat. Res. 167 (2007) 319–329.
[13] H. Nikjoo, S. Uehara, D. Emfietzoglou, F.A. Cucinotta, Track-structure codes in radiation research, Radiat. Meas. 41 (2006) 1052–1074.
[14] V.A. Semenenko, R.D. Stewart, Fast Monte Carlo simulation of DNA damage formed by electrons and light ions, Phys. Med. Biol. 51 (2006) 1693–1706.

[15] S. Uehara, H. Nikjoo, Monte Carlo simulation of water radiolysis for low-energy charged particles, J. Radiat. Res. 47 (2006) 69–81.
[16] B. Aydogan, W.E. Bolch, S.G. Swarts, J.E. Turner, D.T. Marshall, Monte Carlo simulations of site-specific radical attack to DNA bases, Radiat. Res. 169 (2008) 223–231.
[17] B. Grosswendt, S. Pszona, The track structure of α-particles from the point of view of ionization-cluster formation in "nanometric" volumes of nitrogen, Radiat. Environ. Biophys. 41 (2002) 91–102.
[18] B. Aydogan, D.T. Marshall, S.G. Swarts, J.E. Turner, A.J. Boone, N.G. Richards, W.E. Bolch, Site-specific OH attack to the sugar moiety of DNA: a comparison of experimental data and computational simulation, Radiat. Res. 157 (2002) 38–44.
[19] H. Date, K.L. Sutherland, H. Hasegawa, M. Shimozuma, Ionization and excitation collision processes of electrons in liquid water, Nucl. Instr. Meth. B 265 (2007) 515–520.
[20] ICRU Report 37. 1984. Stopping powers of electrons and positrons. International Commission on Radiation Units and Measurements. Washington, DC, Vol. 37.
[21] ORNL/TM-10851. 1988. Monte Carlo Simulation of Indirect Damage to Biomolecules Irradiated in Aqueous Solution – The Radiolysis of Glycylglycine. Oak Ridge National Laboratory, Martin Marietta Energy Systems, Inc.
[22] S.M. Pimblott, J.A. LaVerne, A. Mozumder, Monte Carlo simulation of range and energy deposition by electrons in gases and liquid water, J. Phys. Chem. 100 (1996) 8595–8606.
[23] J.E. Turner, R.N. Hamm, M.L. Souleyrette, D.E. Martz, T.A. Rhea, D.W. Schmidt, Calculations for β dosimetry using Monte Carlo Code (OREC) for electron transport in water, Health Phys. 55 (1998) 741–750.
[24] H. Date, Y. Yoshii, K.L. Sutherland, Nanometer site analysis of electron tracks and dose localization in bio-cells exposed to X-ray irradiation, Nucl. Instr. Meth. B 267 (2009) 1135–1138.
[25] B. Grosswendt, E. Waibel, Transport of low energy electrons in nitrogen and air, Nucl. Instr. and Meth. 155 (1978) 145–156.
[26] M. Terrissol, A. Beaudré, Simulation of space and time evolution of radiolytic species induced by electrons in water, Radiat. Prot. Dosim. 31 (1990) 175–177.
[27] R. Roots, S. Okada, Estimation of life times and diffusion distances of radicals involved in X-ray-induced DNA strand breaks or killing of mammalian cells, Radiat. Res. 64 (1975) 306–320.
[28] W.R. Holley, I.S. Mian, S.J. Park, B. Rydberg, A. Chatterjee, A model of interphase chromosomes and evaluation of radiation-induced aberrations, Radiat. Res. 158 (2002) 568–580.
[29] M. Beuve, A. Colliaux, D. Dabli, D. Dauvergne, B. Gervais, G. Montarou, E. Testa, Statistical effects of dose deposition in track-structure modelling of radiobiology efficiency, Nucl. Instr. Meth. B 267 (2009) 983–988.
[30] L.E. Feinendegen, The cell dose concept; potential application in radiation protection, Phys. Med. Biol. 35 (1990) 597–612.
[31] W. Friedland, P. Jacob, H.G. Paretzke, S. Tobias, Monte Carlo simulation of the production of short DNA fragments by low-linear energy transfer radiation using higher-order DNA models, Radiat. Res. 150 (1998) 170–182.
[32] B. Grosswendt, Nanodosimetry, from radiation physics to radiation biology, Radiat. Prot. Dosim. 115 (2005) 1–9.
[33] E.P. Rogakou, D.R. Pilch, A.H. Orr, V.S. Ivanova, W.M. Bonner, DNA double-stranded breaks induce histone H2AX phosphorylation on serine 139, J. Biol. Chem. 273 (1998) 5858–5868.
[34] K. Rothkamm, M. Löbrich, Evidence for a lack of DNA double-strand break repair in human cells exposed to very low X-ray doses, PNAS 100 (2003) 5057–5062.
[35] S. Bekker-Jensen, C. Lukas, F. Melander, J. Bartek, J. Lukas, Dynamic assembly and sustained retention of 53BP1 at the sites of DNA damage are controlled by Mdc1/NFBD1, J. Cell Biology 170 (2005) 201–211.
[36] F. Pryde, S. Khalili, K. Robertson, J. Selfridge, A.M. Ritchie, D.W. Melton, D. Jullien, Y. Adachi, 53BP1 exchanges slowly at the sites of DNA damage and appears to require RNA for its association with chromatin, J. Cell Science 118 (2005) 2043–2055.
[37] B. Jakob, J. Splinter, G. Taucher-Scholz, Positional stability of damaged chromatin domains along radiation tracks in mammalian cells, Radiat. Res. 171 (2009) 405–418.
[38] N. Bhogal, F. Jalali, R.G. Bristow, Microscopic imaging of DNA repair foci in irradiated normal tissue, Int. J. Radiat. Biol. 85 (2009) 732–746.
[39] H. Date, K.L. Sutherland, T. Hayashi, Y. Matsuzaki, Y. Kiyanagi, Inelastic collision processes of low-energy protons in liquid water, Radiat. Phys. and Chem. 75 (2006) 179–187.
[40] K. Wiklund, G.H. Olivera, A. Brahme, B.K. Lind, Radial secondary electron dose profiles and biological effects in light-ion beams based on analytical and Monte Carlo calculations using distorted wave cross sections, Radiat. Res. 170 (2008) 83–92.